# Noise Parameter Optimization of UHV/CVD SiGe HBT's for RF and Microwave Applications

Guofu Niu, *Member, IEEE*, William E. Ansley, Shiming Zhang, *Student Member, IEEE*, John D. Cressler, *Senior Member, IEEE*, Charles S. Webster, and Robert A. Groves, *Member, IEEE*

***Abstract*—This paper demonstrates a predictive noise parameter estimation methodology for UHV/CVD SiGe HBT's which combines ac measurement, calibrated ac simulation and two of the latest $Y$-parameter-based noise models: 1) the thermodynamic noise model, and 2) the SPICE noise model. The bias current and frequency dependence of the minimum noise figure, the optimum generator admittance, and the noise resistance are calculated using both models and compared with measurements. The observed agreements and discrepancies are investigated using circuit analysis of the chain noisy two-port representation. For the devices under study, the SPICE model description of thermal noise produces a better overall agreement to data in terms of all the noise parameters. Experiments on devices with different collector doping levels show that both low noise and high breakdown voltage can be realized with one profile without significantly compromising the ac current gain and the ac power gain.**

***Index Terms*—AC simulation, bipolar technology, chain noisy two-port representation, low noise amplifier (LNA), noise figure, SiGe HBT, SPICE, thermodynamic noise model.**

## I. Introduction

FOR low-noise RF and microwave applications, the SiGe transistor profile and layout need to be optimized to achieve a minimum noise figure. Noise measurements in the GHz range require substantial experimental effort, and the optimization of a low-noise device (including layout, doping and Ge profile) through fabrication and measurement iteration can be very expensive and time consuming. The purpose of this work is to explore the feasibility of *predictive* noise parameter estimation in UHV/CVD SiGe HBT's by combining ac numerical simulation and two of the latest $Y$-parameter-based noise models: 1) the thermodynamic noise model [1], and 2) the SPICE noise model [2]. The two-dimensional (2-D) device simulator MEDICI [3] was used in place of ac measurement on fabricated devices, and the simulated $Y$-parameters are subsequently used to calculate the noise parameters using an in-house post-processing program. The device structure including the 2-D doping profile transitions and physical model coefficients was calibrated to ac measurements up to 40 GHz. Although the noise parameters can be calculated from either ac measurements or ac simulation, the use of ac simulation enables specific Ge and doping profile optimization without real time fabrication. A systematic analysis of the difference between the two noise models is performed to gain insight into the results and provide guidelines for practical optimization purposes using simulation. Profile design issues for both low noise and high breakdown voltage applications are also discussed.

## II. Device Technology and Measurement Setup

The SiGe HBT's were fabricated using a self-aligned epitaxial-base technology [4]. Fig. 1 shows a schematic cross section of the device. The SiGe base is formed in an ultrahigh-vacuum/chemical vapor deposition (UHV/CVD) low temperature epitaxy (LTE) system. Polysilicon deposited over the field oxide during the LTE serves as the extrinsic base contact. Polysilicon-filled, closed-bottom, deep trenches isolate adjacent subcollectors, and the field oxide is fabricated using a planar shallow trench process. For standard devices in the technology, the intrinsic collector was formed by a double implantation to realize high performance. Representative vertical doping and Ge profiles of the standard SiGe HBT are shown in Fig. 2. For RF power applications, devices with a higher breakdown voltage were fabricated on the same wafer by leaving out one of the collector implantations [5]. We will refer to the device with a double collector implant, and the single collector implant device, as the "standard" device ($\mathrm{BV_{CEO}} = 3.3$ V) and "high $\mathrm{BV_{CEO}}$" device ($\mathrm{BV_{CEO}} = 5.3$ V), respectively.

DC characteristics were measured on-wafer using an HP4155, and ac characteristics were measured on-wafer using an HP8510C network analyzer. The noise figure of a $0.5 \times 20 \times 2\ \mu\mathrm{m}^2$ standard device was measured from 2 to 18 GHz using an NP-5 on-wafer measurement system from ATN Microwave Inc. A summary of the electrical characteristics is given in Table I.

## III. Noise Models

In most of the SPICE (e.g., HSPICE, PSPICE, or SmartSpice) and harmonic balance simulators (e.g., Libra), the nonlinear noise model for BJT's is described by two shot noise current generators flowing from the base and collector to the emitter and two thermal noise voltage generators at the

Manuscript received October 22, 1998; revised February 26, 1999. This work was supported by IBM under an IBM University Partnership Research Program Award. The review of this paper was arranged by Editor M. F. Chang.

G. Niu, S. Zhang, and J. D. Cressler are with the Alabama Microelectronics Science and Technology Center, Electrical Engineering Department, Auburn University, Auburn, AL 36849 USA.

W. E. Ansley and R. A. Groves are with IBM Microelectronics, Hopewell Junction, NY 12533 USA.

C. S. Webster is with IBM Microelectronics, Essex Junction, VT 05452 USA.

Publisher Item Identifier S 0018-9383(99)05989-4.

0018–9383/99$10.00 © 1999 IEEE

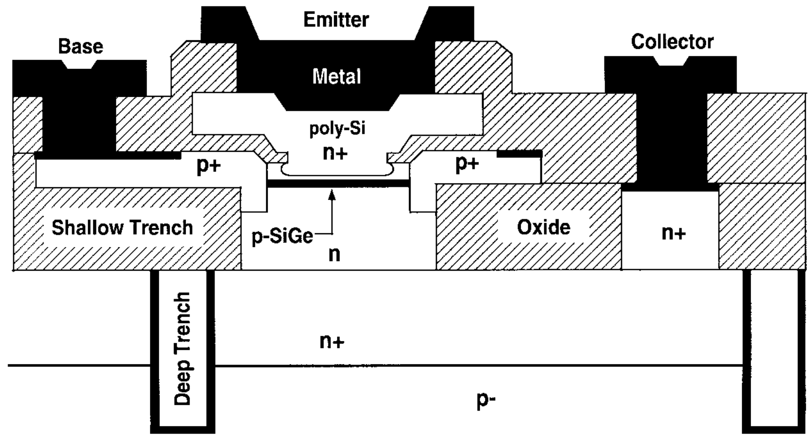


Fig. 1. Schematic cross section of the UHV/CVD SiGe HBT used in this investigation.

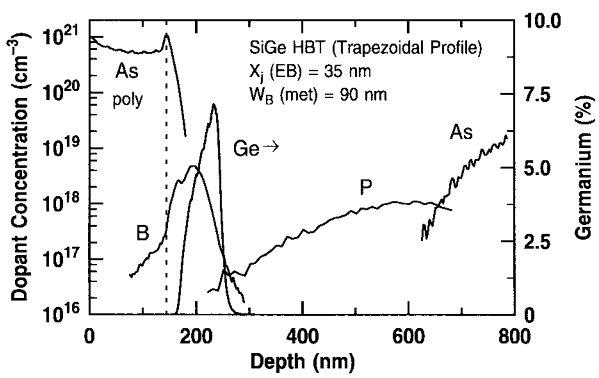


Fig. 2. Representative SIMS doping and Ge profiles of the UHV/CVD SiGe HBT's.

TABLE I
SUMMARY OF DEVICE ELECTRICAL CHARACTERISTICS ($A_E = 0.5 \times 20 \times 2\ \mu m^2$)

| | Standard Device | High $BV_{CEO}$ Device |
|---|---|---|
| Peak $\beta$ | 110 | 95 |
| Peak $f_T$ (GHz) | 51 | 33 |
| Peak $f_{max}$ (GHz) | 64 | 40 |
| $R_B$ (Ω) @ $I_c$=10mA | 8.9 | 10.2 |
| $BV_{CEO}$ (V) | 3.3 | 5.3 |

base and emitter, as shown in Fig. 3. An analytical equation of the minimum noise factor ($F_{\min}$) was derived recently in terms of the $Y$-parameters, the series base resistance $r_B$, and emitter resistance $r_E$ [2] [see (1) and (2), shown at the bottom of the page], where $r_{BE} \equiv r_B + r_E$, and $I_C$ and $I_B$ are collector and base currents, respectively. The base and emitter resistances need to be extracted from experiment or simulation. The optimum generator admittance at which $F_{\min}$ occurs for a given bias point and frequency is given by [2]

$$Y_{G,\text{opt}} = G_{G,\text{opt}} + jB_{G,\text{opt}} \tag{3}$$

where

$$G_{G,\text{opt}} = \sqrt{\frac{I_B|Y_{21}|^2 + I_c|Y_{11}|^2}{\frac{2kT}{q}|Y_{21}|^2 r_{BE} + I_c} - \left(\frac{I_c\,\text{Im}\{Y_{11}\}}{\frac{2kT}{q}|Y_{21}|^2 r_{BE} + I_c}\right)^2} \tag{4}$$

$$B_{G,\text{opt}} = \frac{-\text{Im}\{Y_{11}\}}{\frac{2kT}{q}|Y_{21}|^2 r_{BE}/I_c + 1}. \tag{5}$$

The noise resistance $R_n$ relating to the input-referred noise voltage $\langle v_n^2 \rangle$ is given by [2]

$$\begin{aligned} R_n &\equiv \frac{\langle v_n^2\rangle}{4kT\Delta f} \\ &= \frac{I_c}{\frac{2kT}{q}|Y_{21}|^2} + r_{BE}. \end{aligned} \tag{6}$$

Note that the first part of the input-referred noise voltage comes from the collector shot noise $2qI_C$, and the second part comes from the base and emitter resistances.

The other description of transistor noise is the so-called thermodynamic approach [1]. The shot noise generators are the same as in the SPICE models, however, the thermal noise is represented by an input noise current generator $S_I = 4kT$ Re($Y_{11}$), which is derived from the fluctuation-dissipation theorem or generalized Nyquist expression for two poles near equilibrium [1], as shown in Fig. 4. Note that the thermal noise current generator operates on the whole transistor including parasitic base and emitter resistances and directly relates to the input $Y$-parameters. As a result, the noise parameters can be directly calculated from $Y$-parameters without extracting $r_B$ and $r_E$, which provides significant time saving for the

$$F_{\min} = 1 + \frac{qI_c}{KT|Y_{21}|^2}(\text{Re}\{Y_{11}\} + A) \tag{1}$$

$$A = \sqrt{\left[1 + \frac{2kT|Y_{21}|^2 r_{BE}}{qI_c}\right]\left[|Y_{11}|^2 + \frac{I_B|Y_{21}|^2}{I_c}\right] - (\text{Im}\{Y_{11}\})^2} \tag{2}$$

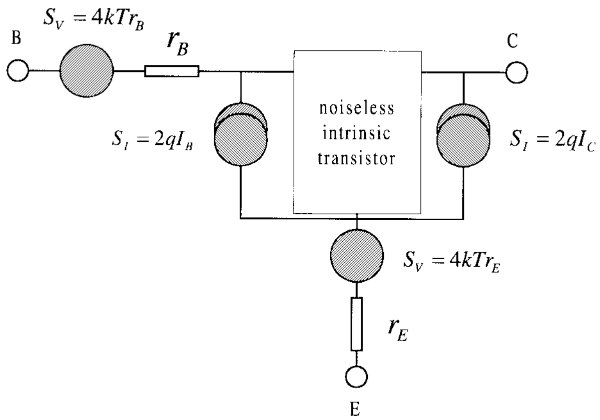


Fig. 3. Schematic of the SPICE noise model. The thermal noise is described by low-voltage noise sources due to the parasitic base and emitter resistance.

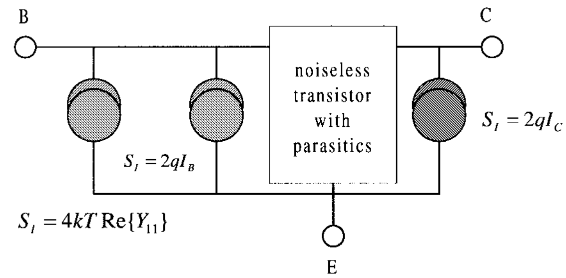


Fig. 4. Schematic of the thermodynamic noise model based on fluctuation-dissipation theorem for two poles near equilibrium. The thermal noise is described by an input current noise source associated with the real part of $Y_{11}$.

optimization of noise figure at a particular frequency. The extraction of $r_B$ and $r_E$ using the impedance circle method requires the simulation of $Y$-parameters at multiple frequencies even if the noise figure is optimized for only a single frequency. The resulting minimum noise factor equation for the thermodynamic model is [6], [7]

$$F_{\min} = 1 + \frac{I_B + \dfrac{2kT}{q}\,\mathrm{Re}\{Y_{11}\} + I_c\left[\dfrac{\mathrm{Re}\{Y_{11}\} + G_{G,\mathrm{opt}}}{|Y_{21}|}\right]^2}{2G_{G,\mathrm{opt}}kT/q} \tag{7}$$

where $G_{G,\mathrm{opt}}$ is the real part of the generator admittance (or source conductance) at minimum noise factor [7]

$$G_{G,\mathrm{opt}} = \sqrt{(\mathrm{Re}\{Y_{11}\})^2 + |Y_{21}|^2\frac{2I_B + 4\,\mathrm{Re}\{Y_{11}\}kT/q}{2I_c}}. \tag{8}$$

The imaginary part of the generator admittance at minimum noise factor is equal to the conjugate of the imaginary part of the input admittance of the transistor [7]

$$B_{G,\mathrm{opt}} = -\mathrm{Im}\{Y_{11}\}. \tag{9}$$

Note that (9) is different from (5). Detailed discussion of why they are different will be given below. The noise resistance $R_n$ relating to the input-referred noise voltage $\langle v_n^2\rangle$ is given by

$$R_n = \frac{I_c}{\dfrac{2kT}{q}|Y_{21}|^2}. \tag{10}$$

Note that the second term in the right hand side of (6) does not exist in (10) because

1) the thermal noise is taken into account through an input current source;
2) the input-referred noise voltage is obtained by short circuiting the input and calculating the input voltage generating equal output noise;
3) and thus, the thermal noise, when described by an input current noise source, does not contribute to the input-referred noise voltage, and hence does not contribute to the noise resistance $R_n$.

Independent of the noise model used, the noise factor for any arbitrary generator admittance $Y_G = G_G + jB_G$ is given by the following universal relation pertaining to a linear noisy two-port [8]:

$$F = F_{\min} + \frac{R_n}{G_G}\,|Y_G - Y_{G,\mathrm{opt}}|^2. \tag{11}$$

Equation (11) forms the basis of noise factor measurement and is widely used in circuit design. The reflection coefficient $\Gamma_{G,\mathrm{opt}}$, instead of the admittance $Y_{G,\mathrm{opt}}$ is often used in noise measurements

$$\Gamma_{G,\mathrm{opt}} = \frac{1 - Y_{G,\mathrm{opt}}Z_0}{1 + Y_{G,\mathrm{opt}}Z_0} \tag{12}$$

where $Z_0$ is the characteristic impedance and equal to 50 Ω here.

## IV. AC Device Simulation

In our approach, the physical model coefficients such as the bandgap narrowing (BGN) parameters in Si and SiGe are first calibrated so that both the measured dc and ac characteristics are reasonably reproduced from simulation. Incomplete ionization was intentionally turned off because of the lack of models for the semiconductor-metal transition effect [9] at high doping levels which are important for the base resistance estimation. At concentrations higher than $10^{18}$ cm$^{-3}$, the impurity band enters into the majority carrier band, so the original concept of separate bands loses meaning, and the dopants are completely ionized. The base majority carrier concentration was severely under-estimated at doping levels above $10^{18}$ cm$^{-3}$ when the incomplete ionization option was turned on. This is particularly important when simulating the "true" SiGe HBT's with an even higher base doping ($10^{19}$ cm$^{-3}$). To the authors' knowledge, no commercial device simulator has built-in models for the semiconductor-metal transition effect. The Philips Unified Mobility Model (PHUMOB) was selected and found to produce sensible results due to its unique consideration of minority carrier mobility. The lateral field dependence of mobility (FLDMOB) was selected to accurately simulate the collector-base junction capacitance because the CB junction electric field is strong enough to cause velocity saturation even at $V_{CB}$ close to 0 V due to the high collector doping required for optimum performance. Bandgap narrowing due to heavy doping was selected due to the high doping levels in HBT's. However, the bandgap narrowing parameters need to be adjusted in accordance with the type of statistics selected

TABLE II
MEDICI COEFFICIENTS USED IN THIS WORK. DEFAULTS ARE USED FOR OTHER PARAMETERS

| | |
|---|---|
| NSRHN ($cm^{-3}$) SiGe | $10^{19}$ |
| NSRHN ($cm^{-3}$) Si | $10^{17}$ |
| NSRHP ($cm^{-3}$) SiGe | $10^{19}$ |
| NSRHP ($cm^{-3}$) Si | $10^{17}$ |
| TAUN0 (second) | $6\times10^{-9}$ |
| TAUP0 (second) | $2\times10^{-9}$ |
| V0.BGN (eV) Si | $5.0858\times10^{-3}$ |
| N0.BGN ($cm^{-3}$) | $1.3\times10^{17}$ |
| CON.BGN | 0.5 |
| V0.BGN (eV) SiGe | $4.1128\times10^{-3}$ |

(Boltzmann or Fermi-Dirac statistics) because of the difference between the apparent bandgap narrowing and the physical bandgap narrowing, as reviewed in [10]. The simulations here were done using Fermi-Dirac statistics. Table II shows the typical MEDICI model coefficients calibrated for the devices under study. Default values were used for those parameters not listed in Table II. The 2-D device structure was constructed based on vertical SIMS profiles taken through the center of the emitter and the extrinsic base. These vertical doping and Ge profiles are kept as is in the simulation and only the parameters for physical models such as bandgap narrowing and the lateral transition of doping profiles were adjusted in the calibration. The purpose is to enable the doping and Ge profile optimization for minimum noise figure using the same set of physical model coefficients calibrated for this technology. A finer grid was generated self-consistently in places with a larger potential gradient, Ge gradient or doping gradient. The lateral transition between extrinsic and intrinsic base was determined by best-fitting the simulated and measured base resistance. The lateral transition between extrinsic and intrinsic collector was determined by best-fitting the simulated and measured collector-base capacitance. The $Y$-parameters are simulated in MEDICI by solving the system of semiconductor transport equations in the frequency domain.

An examination of the two noise factor equations (1) and (7) shows that $F_{\min}$ from both models strongly depend on $Y_{11}$ and $Y_{21}$. Therefore, our model calibration approach is intended to reproduce not only the cutoff frequency and maximum oscillation frequency, as is the typical approach for model calibration, but also each individual $Y$-parameter. Although there are many 2-D simulation parameters that one can adjust, determining a single set of simulation parameters that can reproduce the four complex network parameters at all the biases of interest (0.1–1.0 mA/$\mu$m$^2$) for frequencies up to 40 GHz requires substantial effort. An in-depth understanding of the interaction of physics of the simulation models and device operation is especially important for achieving sensible results. For instance, at lower current, the total transit time is dominated by the time constants relating to the EB space charge region capacitance rather than the diffusion capacitance. Therefore, the adjustment of mobility parameters in the base affects only the cutoff frequency at higher current level and does not help the lower current level calibration. On the contrary, the peak cutoff frequency value and its roll-off due to the Kirk effect are mainly determined by the time constants relating to the EB diffusion capacitance and hence mobility parameters, as well as the velocity saturation parameters.

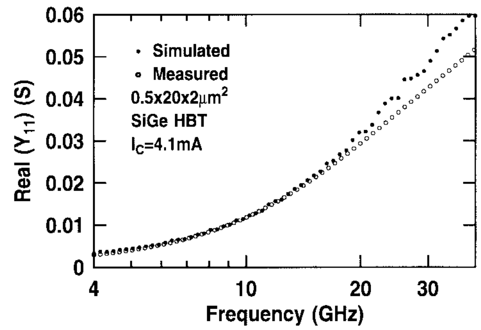


Fig. 5. Comparison of simulated and measured real part of $Y_{11}$, which enters into the $NF_{\min}$ equations for both the SPICE noise model and the thermodynamic noise model ($I_C = 4.1$ mA and $A_E = 0.5 \times 20 \times 2\ \mu\text{m}^2$).

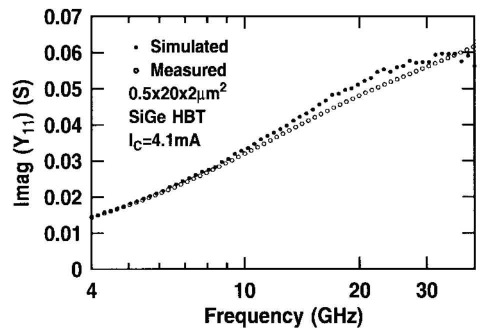


Fig. 6. Comparison of simulated and measured imaginary part of $Y_{11}$, which enters into the SPICE noise model $NF_{\min}$ equation (1) ($I_C = 4.1$ mA and $A_E = 0.5 \times 20 \times 2\ \mu\text{m}^2$).

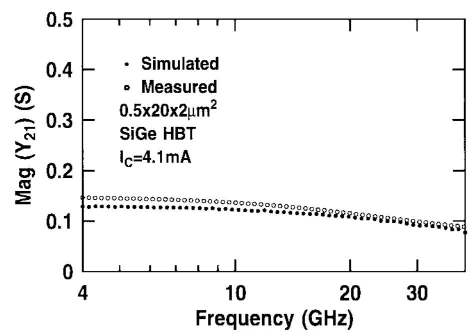


Fig. 7. Comparison of measured and simulated magnitude of $Y_{21}$, which enters into the $NF_{\min}$ equations for both the SPICE noise model and the thermodynamic noise model ($I_C = 4.1$ mA and $A_E = 0.5 \times 20 \times 2\ \mu\text{m}^2$).

Figs. 5–7 show the comparison of the simulated and measured real part of $Y_{11}$, the imaginary part of $Y_{11}$, and the magnitude of $Y_{21}$ versus frequency at $I_C = 4.1$ mA for a $0.5 \times 20 \times 2\ \mu\text{m}^2$ SiGe HBT. These three parameters closely relate to the noise parameters in the SPICE noise model, as can be seen from (1). Two of these parameters (Re $\{Y_{11}\}$ and Mag $\{Y_{21}\}$) closely relate to the noise parameters in the thermodynamic model. The calibrated simulation agrees well with measurement for all the three $Y$-parameters, particularly below 20 GHz, and therefore can be used for further noise parameter estimation.

## V. Simulation of Noise Parameters

Having verified the accuracy of the calibrated 2-D simulation, we proceed with the calculation of the noise parameters using the simulated $Y$-parameters. Results from both noise models are compared to the measured data to explore their differences. For a complete verification, we examine the current and frequency dependence of all of the three noise parameters including the minimum noise factor $F_{\min}$ (through the minimum noise figure $NF_{\min} = 10\log(F_{\min})$), the optimum admittance $Y_{G,\mathrm{opt}}$ (through $\Gamma_{G,\mathrm{opt}}$), and the noise resistance $R_n$.

### A. The Minimum Noise Factor $F_{\min}$ (Through Minimum Noise Fig. $NF_{\min} = 10\log F_{\min}$)

First, the base and emitter resistance needs to be extracted for the SPICE noise model. In [2], the base and emitter resistances were determined separately using the averaged real part of $Z_{11} - Z_{12}$ and $Z_{12}$ at frequencies below 1 GHz. We observe here that the sum of the base and emitter resistances $r_{BE}(r_{BE} \equiv r_B + r_E)$, which enters into the noise parameter equation of the SPICE noise model, can be directly determined from the left intercept of the semi-circle on the complex plane of the input impedance. Using a 50-$\Omega$ characteristic impedance, the input impedance high-frequency intercept is readily obtained from the equivalent circuit in Fig. 3 by shorting all the three internal terminals of the intrinsic transistor

$$\begin{aligned} Z_{\mathrm{in}} &= r_B + r_E // 50\ \Omega \\ &\approx r_B + r_E \end{aligned} \tag{13}$$

because the emitter resistance is usually far less than 50 Ω. In best fitting the simulated input impedance, the low-frequency data are favored against the high-frequency data because the lumped equivalent circuit description of transistor operation is no longer accurate at very high frequencies.

Figs. 8 and 9 show the simulated and measured minimum noise figure $(NF_{\min} = 10\log\ F_{\min})$ versus collector current at 2 and 10 GHz, respectively. The agreement between simulation using both noise models and measurement is close at 10 GHz. At 2 GHz, for the operating current where the $NF_{\min}$ is minimum, the agreement between simulation and measurement is also close. Fig. 10 shows the simulated minimum noise figure versus frequency at $I_C = 1.26$ mA, a relatively low current value giving the minimum $NF_{\min}$. Considering the on-wafer noise measurement accuracy, the agreement between simulation and measurement is excellent across 2–18 GHz, a frequency range at which these SiGe HBT's are best suited to operate. This indicates that both $Y$-parameter-based noise models can be used in this low current density region which is of practical interest for $NF_{\min}$ and that such an ac simulation-noise model approach can be used for predictive noise figure optimization.

### B. The Optimum Generator Admittance $Y_{G,\mathrm{opt}}$ ($\Gamma_{G,\mathrm{opt}}$)

The other important noise parameter is the optimum generator admittance $Y_{G,\mathrm{opt}}$, which is often characterized by the reflection coefficient at minimum noise figure $(\Gamma_{G,\mathrm{opt}})$ in

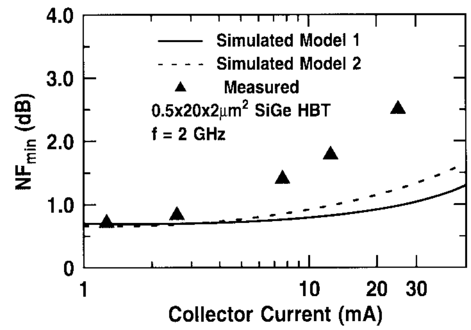


Fig. 8. Comparison of measured and simulated noise figure versus collector current using both noise models at 2 GHz.

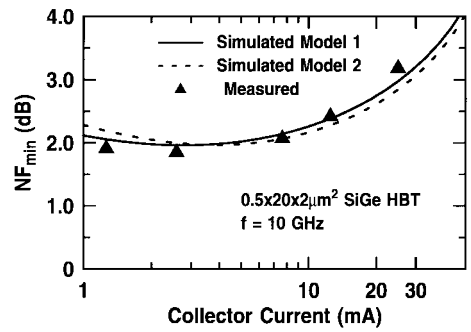


Fig. 9. Comparison of measured and simulated noise figure versus collector current using both noise models at 10 GHz.

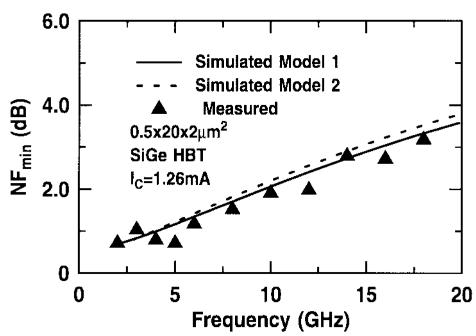


Fig. 10. Comparison of measured and simulated noise figure versus frequency at $I_C = 1.26$ mA.

measurement. Given that both models give $NF_{\min}$ values reasonably close to the data, it is interesting to see how the optimum admittance $Y_{G,\mathrm{opt}}$ compares to the measured data. Figs. 11 and 12 show the magnitude and angle of the optimum reflection coefficient $\Gamma_{G,\mathrm{opt}}$ [defined in (12)] versus collector current at 2 GHz, and Figs. 13 and 14 show the same comparisons at 10 GHz. Although the qualitative behavior is similar for the two models, the SPICE noise model shows a closer agreement to the measured data, particularly at 2 GHz. This indicates that for the devices under study, the physical description of thermal noise in the SPICE model is more appropriate. Figs. 15 and 16 show the magnitude and angle of the $\Gamma_{G,\mathrm{opt}}$ versus frequency at $I_C = 1.26$ mA, a relatively low current value giving the minimum $NF_{\min}$ at all the frequencies of interest. At such low currents, comparable to those in low-noise amplifier applications, both models can reasonably reproduce the measured optimum admittance. Therefore, from a simulation perspective, the thermodynamic model is still preferred in low-noise device design at low current for a

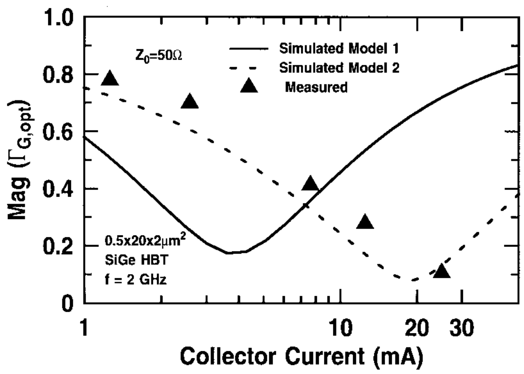


Fig. 11. Comparison of measured and simulated magnitude of the optimum reflection coefficient versus collector current using both noise models at 2 GHz.

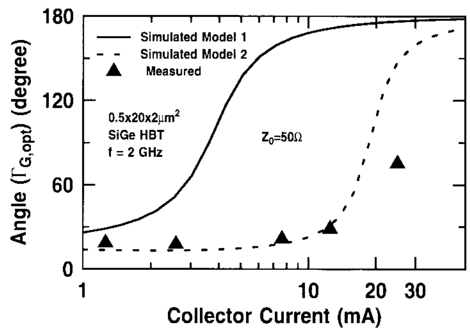


Fig. 12. Comparison of measured and simulated angle of the optimum reflection coefficient versus collector current using both noise models at 2 GHz.

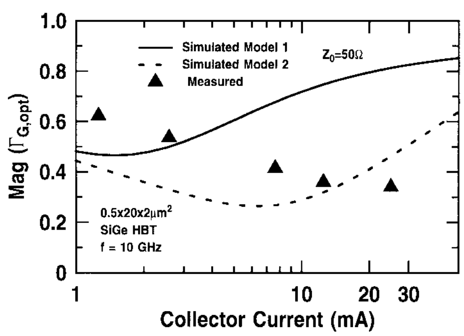


Fig. 13. Comparison of measured and simulated magnitude of the optimum reflection coefficient versus collector current using both noise models at 10 GHz.

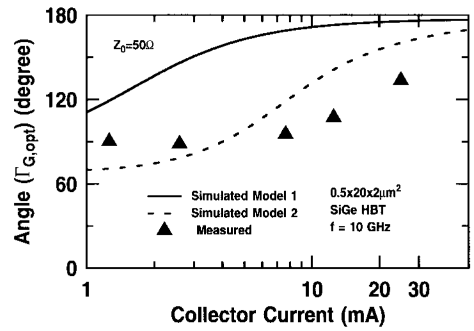


Fig. 14. Comparison of measured and simulated angle of the optimum reflection coefficient versus collector current using both noise models at 10 GHz.

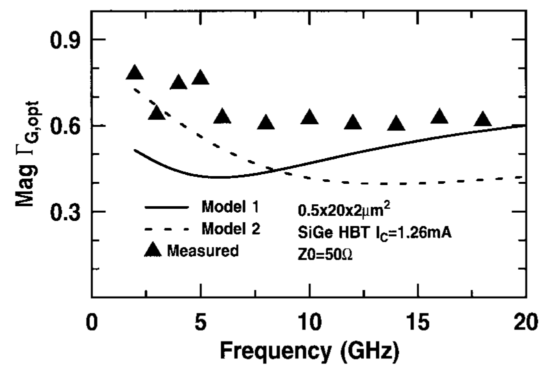


Fig. 15. Comparison of measured and simulated magnitude of the optimum reflection coefficient versus frequency at $I_C = 1.26$ mA using both noise models.

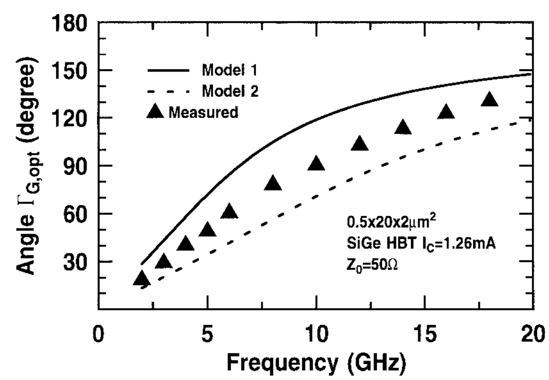


Fig. 16. Comparison of measured and simulated angle of the optimum reflection coefficient versus frequency at $I_C = 1.26$ mA using both noise models.

given frequency. The SPICE model, however, needs the base resistance, the extraction of which requires a semi-circle in the input-impedance plane, and hence requires simulation at multiple frequencies. However, if the application requires higher operation current, the SPICE model needs to be used for an accurate source matching network design.

### C. The Noise Resistance $R_n$

The associated gain of a device at minimum noise figure may not be sufficient for application as a low-noise amplifier. In this situation, a compromise between input matching for minimum noise figure and for power gain can be made. The noise resistance $R_n$ determines the sensitivity of the total noise figure to deviations from optimum noise admittance matching $Y_{G,\mathrm{opt}}$, as can be seen in (11). According to the linear two-port noise theory, $R_n$ can be determined by the input-referred noise voltage $\langle v_n^2\rangle$ using (6). Because of the difference in thermal noise consideration, $\langle v_n^2\rangle$ for the thermodynamic model is due to the $2qI_C$ shot noise only, while the $\langle v_n^2\rangle$ for the SPICE model has an extra contribution from the base and emitter resistance. Although the two noise models yielded similar $NF_{\min}$ and $Y_{G,\mathrm{opt}}$ at low currents of interest to minimum noise figure, they gave very different equations of $R_n$. A comparison of $R_n$ from both models with the measurement data will provide further insight into the model differences. Figs. 17 and 18 show the $R_n$ comparison between models and measurement as a function of bias current at 2 and 10 GHz. Fig. 19 shows the $R_n$ comparison as a function of frequency.

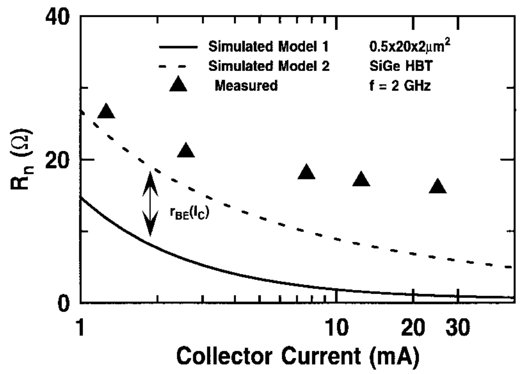


Fig. 17. Comparison of measured and simulated noise resistance versus collector current using both noise models at 2 GHz.

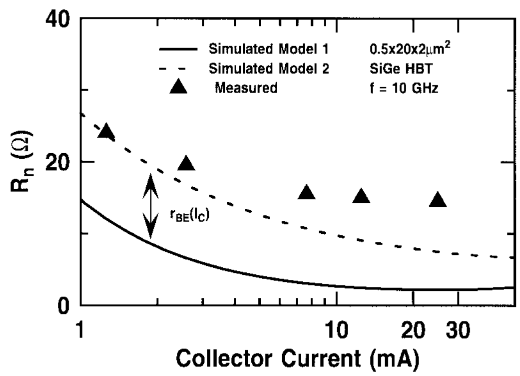


Fig. 18. Comparison of measured and simulated noise resistance versus collector current using both noise models at 10 GHz.

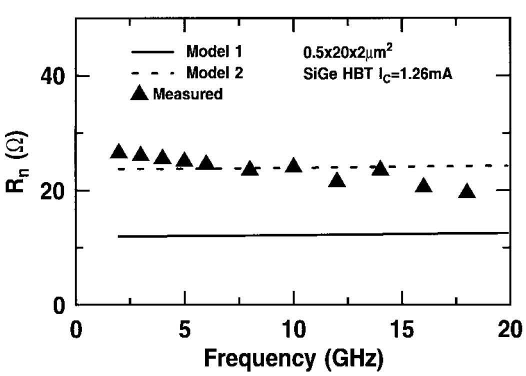


Fig. 19. Comparison of measured and simulated noise resistance versus frequency using both noise models at $I_C = 1.26$ mA.

The SPICE model is in close agreement with the measured $R_n$, which also suggests that the description of thermal noise through the base and emitter resistance is more suitable for the SiGe HBT's used in this work. From a practical point of view, $R_n$ is not important if the device is to operate at noise matching for minimum noise figure. Therefore, the thermodynamic model can still be used for profile optimization due to its low simulation cost discussed earlier. After the design goal for minimum noise factor is achieved, the SPICE model can be used to obtain the optimum admittance and noise resistance. Specific Ge and doping profile optimization for the design of a microwave SiGe HBT with a 2-dB noise figure, and 15 dB associated gain at noise matching for 20 GHz operation using this ac 2-D simulation-noise model approach, will be reported in a separate paper.

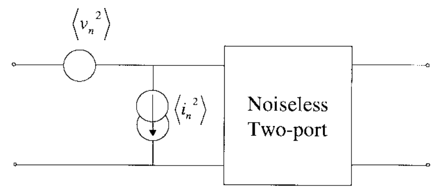


Fig. 20. Circuit schematic of the chain noisy two-port representation.

### *D. Further Probing of the Relations Between the Two Models*

Despite a very different consideration of the thermal noise, the traditional SPICE noise model and the thermodynamic noise model lead to nearly identical minimum noise figure and optimum noise matching admittance at low current in the devices under study. The noise resistance, however, differs by the amount of base and emitter resistance between the two models. An interesting question is how to understand the observed agreements and discrepancies. The essential differences between two models are two-fold: 1) The thermal noise source in the SPICE model is determined by the series resistance, while the thermal noise source in the thermodynamic model is determined by the real part of input $Y$ parameter $(Y_{11})$. 2) The thermal noise in the SPICE model is represented by a voltage source in series with the input voltage, while the thermal noise in the thermodynamic model is represented by a current source in parallel with the input current. These differences can be used to explain the observations, as described below.

Any noisy network can be replaced by a chain noise equivalent circuit, which consists of the original two-port (assumed to be noiseless), the correlated input-referred current noise source $\langle i_n^2\rangle$, and the input-referred voltage noise source $\langle v_n^2\rangle$ [8], as shown in Fig. 20. Independent of the physical sources of noises inside the device, the four noise parameters can be expressed as a function of $\langle i_n^2\rangle$, $\langle v_n^2\rangle$, and their cross-correlation $\langle v_n i_n^*\rangle$ [8], [11], [12]

$$F_{\min} = 1 + 2(C_r + \sqrt{R_n G_n - C_i^2}) \tag{14}$$

$$G_{G,\text{opt}} = \sqrt{\frac{G_n}{R_n} - \left(\frac{C_i}{R_n}\right)^2} \tag{15}$$

$$B_{G,\text{opt}} = \frac{C_i}{R_n} \tag{16}$$

$$R_n = \frac{\langle v_n^2\rangle}{4kT\Delta f} \tag{17}$$

where

$$G_n = \frac{\langle i_n^2\rangle}{4kT\Delta f} \tag{18}$$

$$C_r = \frac{\text{Re}\{\langle v_n i_n^*\rangle\}}{4kT\Delta f} \tag{19}$$

$$C_i = \frac{\text{Im}\{\langle v_n i_n^*\rangle\}}{4kT\Delta f}. \tag{20}$$

Table III gives the comparison of $\langle i_n^2\rangle$, $\langle v_n^2\rangle$, and the cross-correlation $\langle v_n i_n^*\rangle$ for the two models obtained by transforming the two noisy two-ports in Figs. 3 and 4 to their chain noisy two-ports through circuit analysis. Details of the circuit analysis are omitted for space limitation. $\langle i_n^2\rangle$ is obtained by open circuiting the input and dividing the output noise

TABLE III
COMPARISON OF $\langle i_n^2 \rangle$, $\langle v_n^2 \rangle$, AND $\langle v_n i_n^* \rangle$ BETWEEN THE TWO NOISE MODELS

| | Thermodynamic Model | SPICE Model |
|---|---|---|
| $< i_n^2 >$ | $4kT\,\mathrm{Re}\{Y_{11}\} + 2qI_B + \frac{2qI_C\lvert Y_{11}\rvert^2}{\lvert Y_{21}\rvert^2}$ | $2qI_B + \frac{2qI_C\lvert Y_{11}\rvert^2}{\lvert Y_{21}\rvert^2}$ |
| $< v_n^2 >$ | $\frac{2qI_C}{\lvert Y_{21}\rvert^2}$ | $4kTr_{BE} + \frac{2qI_C}{\lvert Y_{21}\rvert^2}$ |
| $< v_n i_n^* >$ | $\frac{2qI_C Y_{11}^*}{\lvert Y_{21}\rvert^2}$ | $\frac{2qI_C Y_{11}^*}{\lvert Y_{21}\rvert^2}$ |

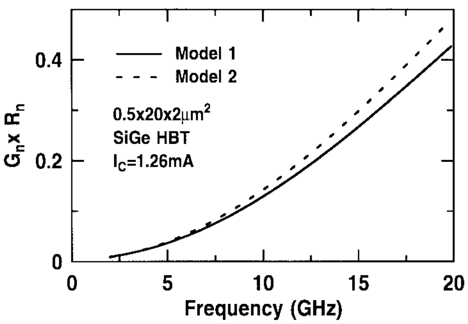


Fig. 21. Comparison of the $R_n G_n$ product calculated using the two models.

current by $|H_{21}|^2$, which is $|Y_{21}/Y_{11}|^2$ by definition. $\langle v_n^2 \rangle$ is obtained by short circuiting the input and dividing the output noise current by $|Y_{21}|^2$. The cross-correlation $\langle v_n i_n^* \rangle$ is then calculated using the internal noise sources common to both $i_n$ and $v_n$, which is the collector shot noise $2qI_C$ in both models.

A careful inspection of the circuit analysis results reveals the following important relations between the two models.

1) The cross-correlation $\langle v_n i_n^* \rangle$ and hence $C_r$ and $C_i$ are the same for both models.
2) $\langle i_n^2 \rangle$ is the same for both models except for an extra term $4kT$ Re $\{Y_{11}\}$ in the thermodynamic model.
3) $\langle v_n^2 \rangle$ is the same for both models except for an extra term $4kTr_{BE}$ in the SPICE model.
4) The product of $\langle i_n^2 \rangle$ and $\langle v_n^2 \rangle$, which determines the $G_n R_n$ product, share two common terms.

Consequently, the difference in $R_n$, $G_{G,\mathrm{opt}}$, and $B_{G,\mathrm{opt}}$ between the two models can be readily understood from the difference in $\langle v_n^2 \rangle$, $\langle i_n^2 \rangle$. The minimum noise figure is expected to differ only by the $G_n R_n$ product, as can be seen from (14). Although $G_n$ and $R_n$ are very different for the two models, their product $G_n R_n$, which shares two common terms, could be similar. In that case, similar $NF_{\min}$ values are obtained using both models despite the difference in $Y_{G,\mathrm{opt}}$ and $R_n$. Fig. 21 compares the $G_n R_n$ product calculated using both models at $I_C = 1.26$ mA. The two models give a similar $G_n R_n$ product, which is responsible for the agreement in $NF_{\min}$ shown in Fig. 10.

The thermodynamic model noise factor expression, (7), which was originally derived using the independent internal noise sources [1], can also be derived by substituting the $\langle v_n^2 \rangle$, $\langle i_n^2 \rangle$, and $\langle v_n i_n^* \rangle$ in Table III into the general-purpose noise figure equation for the chain noisy network representation (14). The derivation using the chain noisy two-port is more complex than the original derivation because of the inclusion of the cross-correlation term. However, the chain noisy two-port representation provides a means of comparing models with different physical consideration of the internal noise sources. Comparisons with measurement are also made easier using the chain noisy two-port representation because of the explicit relation between the noise parameters and the noise sources $\langle v_n^2 \rangle$, $\langle i_n^2 \rangle$, and $\langle v_n i_n^* \rangle$.

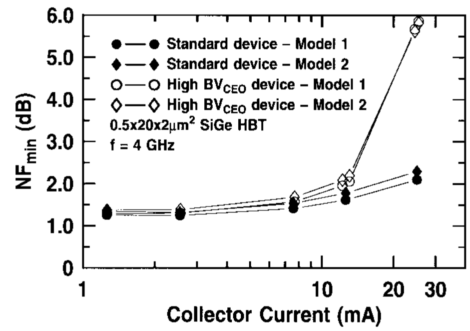


Fig. 22. $NF_{\min}$ versus $I_C$ of the standard device and the high $\mathrm{BV_{CEO}}$ device calculated from measured $Y$-parameters at 4 GHz.

## VI. IMPACT OF COLLECTOR DOPING

A higher breakdown voltage device for power amplifier applications can be achieved in this SiGe technology by leaving out one of the collector implantations. A logical question is: how does the collector profile affect the resultant noise figure? Having verified that the two noise models are accurate at the low-current density of interest for this technology, we have calculated the noise figure of the higher breakdown device ($\mathrm{BV_{CEO}} = 5.3$ V) using the two noise models and measured $S$-parameters. Comparisons to the standard device ($\mathrm{BV_{CEO}} = 3.3$ V) at 4 and 10 GHz are shown in Figs. 22 and 23, respectively. Interestingly, the resulting noise figures from both models are nearly identical to the standard device with a double collector implantation for $I_C < 10$ mA, the bias range which is of practical interest. This implies that as far as noise figure is concerned, the higher breakdown device should provide almost the same performance as the standard device. To better understand this result, Figs. 24 and 25 show the other two high-frequency figures-of-merit, transition frequency $(f_T)$, and maximum oscillation frequency $(f_{\max})$, respectively, versus collector current for the standard and high $\mathrm{BV_{CEO}}$ device. In the current range where $NF_{\min}$ is lowest ($I_C < 10$ mA), the $f_T$ and $f_{\max}$ of the high $\mathrm{BV_{CEO}}$ device are comparable to that of the standard device. Therefore, the high $\mathrm{BV_{CEO}}$ device provides comparable ac current and power gains and may provide profile leverage in circuits that require not only low noise but also higher breakdown voltage.

## VII. CONCLUSIONS

Predictive noise figure calculation in UHV/CVD SiGe HBT's which combines calibrated ac 2-D simulation and $Y$-parameter-based noise models has been demonstrated. A complete comparison of both models with measurement is made for the minimum noise figure, optimum generator admittance, and noise resistance. The observed agreements and discrepancies between the two noise models are explored by comparative circuit analysis of the chain noisy two-ports

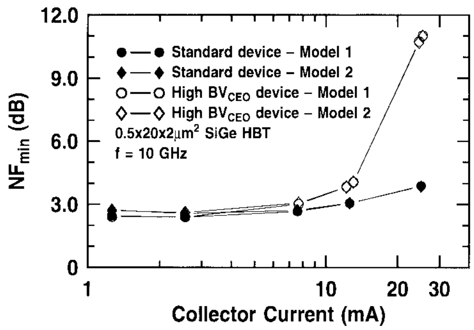


Fig. 23. $NF_{\min}$ versus $I_C$ of the standard device and the high $\mathrm{BV_{CEO}}$ device calculated from measured $Y$-parameters at 10 GHz.

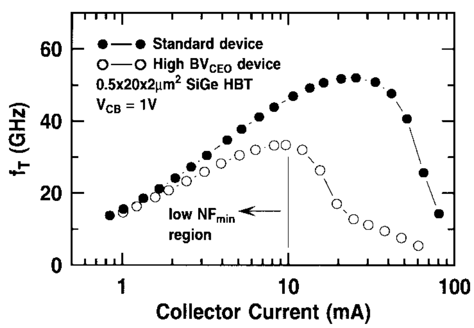


Fig. 24. Measured $f_T$ versus $I_C$ of the standard device and the high $\mathrm{BV_{CEO}}$ device.

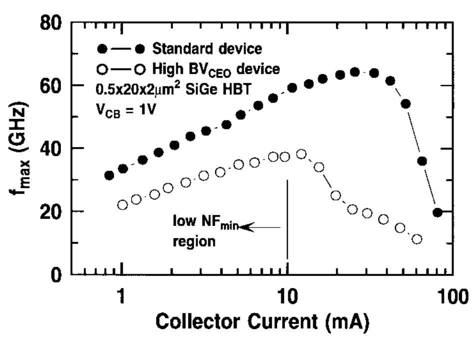


Fig. 25. Measured $f_{\max}$ versus $I_C$ of the standard device and the high $\mathrm{BV_{CEO}}$ device.

for both models. Experiments show that both low noise and high breakdown voltage can be achieved within one profile at relatively low currents without sacrificing ac current gain and ac power gain.

## ACKNOWLEDGMENT

The authors are indebted to D. Ahlgren, D. Harame, S. Subbanna, J. Moniz, A. J. Joseph, B. Meyerson, U. Gogineni, and S. Mathew for their support of this work. G. Niu thanks F. Herzel for the stimulating e-mail exchanges on the thermodynamic noise model throughout this work. They would also like to thank the reviewers for helpful comments and suggestions. The wafers were fabricated at IBM Microelectronics, East Fishkill, NY.

## REFERENCES

[1] F. Herzel and B. Heinemann, "High frequency noise of bipolar devices in consideration of carrier heating and low temperature effects," *Solid-State Electron.*, vol. 38, pp. 1905–1909, Nov. 1995.

[2] S. P. Voinigescu, M. C. Maliepaard, J. L. Showell, G. E. Babcock, D. Marchesan, M. Schroter, P. Schvan, and D. L. Harame, "A scalable high-frequency noise model for bipolar transistors with application to optimal transistor sizing for low-noise amplifier design," *IEEE J. Solid-State Circuits*, vol. 32, pp. 1430–1438, Sept. 1997.

[3] MEDICI, 2-D Semiconductor Device Simulator, Ver. 4.0, Technol. Model. Assoc., Palo Alto, CA, 1997.

[4] D. L. Harame, J. H. Comfort, J. D. Cressler, E. F. Crabbé, J. Y. C. Sun, B. S. Meyerson, and T. Tice, "Si/SiGe epitaxial-base transistors—Part I: Materials, physics, and circuits," *IEEE Trans. Electron Devices*, vol. 42, pp. 469–482, Mar. 1995.

[5] D. C. Ahlgren, G. Freeman, S. Subbanna, R. Groves, D. Greenberg, J. Malinowski, D. Nguyen-Ngoc, S. J. Jeng, K. Stein, K. Schonenberg, D. Kiesling, B. Martin, S. Wu, D. L. Harame, and B. Meyerson, "A SiGe HBT BiCMOS technology for mixed signal RF applications," in *Proc. IEEE BCTM*, Sept. 1997, pp. 195–198.

[6] U. Zillmann and F. Herzel, "An improved SPICE model for high frequency noise of BJT's and HBT's," *IEEE J. Solid-State Circuits*, vol. 31, pp. 1344–1346, Sept. 1996.

[7] F. Herzel, P. Schley, B. Heinemann, U. Zilmann, D. Knoll, D. Temmler, and U. Erben, "Experimental verification and numerical application of the thermodynamic approach to high frequency noise in SiGe HBT's," *Solid-State Electron.*, vol. 41, pp. 387–390, Mar. 1997, and private communications with F. Herzel.

[8] H. A. Haus, W. R. Atkinson, W. H. Fonger, W. W. Mcleod, G. M. Branch, W. A. Harris, E. K. Stodola, W. B. Davenport, Jr., S. W. Harrison, and T. E. Talpey, "Representation of noise in linear twoports," *Proc. IRE*, vol. 48, pp. 69–74, Jan. 1960.

[9] W. Kuzmicz, "Ionization of impurities in silicon," *Solid-State Electron.*, vol. 29, pp. 1223–1227, 1986.

[10] C. M. Van Vliet, "Bandgap narrowing and emitter efficiency in heavily doped emitter structures revisited," *IEEE Trans. Electron Devices*, vol. 40, pp. 1140–1147, June 1993.

[11] H. Hillbrand and P. H. Russer, "An efficient method for computer aided noise analysis of linear amplifier networks," *IEEE Trans. Circuits Syst*, vol. CAS-23, pp. 235–238, Apr. 1976.

[12] L. Escotte, J. Roux, R. Plana, J. Graffeuil, and A. Gruhle, "Noise modeling of microwave heterojunction bipolar transistors," *IEEE Trans. Electron Devices*, vol. 42, pp. 883–888, May 1995.

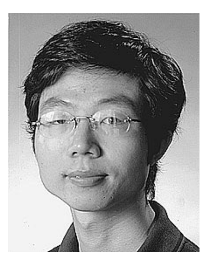

**Guofu Niu** (M'98) was born in Henan, China, in December 1971. He received the B.S., M.S., and Ph.D. degrees in electrical engineering from Fudan University, China, in 1992, 1994, and 1997, respectively. His doctoral research concerned the development of 2-D numerical simulator and physical models for silicon-germanium (SiGe) heterostructure MOSFET's.

In December 1995, he joined the City University of Hong Kong, where he worked on the application of network parallel computing in electronics CAD and the circuit simulation of switched-current oscillators and programmable logic gates utilizing resonant tunneling devices. Since May 1997, he has been with Auburn University, Auburn, AL, working on SiGe RF and microwave devices and circuits, low frequency and broadband noise, inter-modulation characteristics, reliability, nuclear and space radiation effects, SiC power devices, and TCAD as a Post-Doctoral Research Fellow. He has published more than 20 technical journal papers and more than 20 conference papers in the area of microelectronic devices and circuits.

Dr. Niu served on the Program Committee of Asia-South-Pacific Design Automation Conference (ASP-DAC) in 1997, and served as a Technical Reviewer for IEEE ELECTRON DEVICE LETTERS, IEEE TRANSACTIONS ON ELECTRON DEVICES, IEEE JOURNAL OF SOLID-STATE CIRCUITS, and *Solid-State Electronics.*

**William E. Ansley** was born in Naples, FL, on September 11, 1965. He received the B.E.E. degree in 1991, the M.S. degree in 1994, and the Ph.D. degree in 1998, all in electrical engineering from Auburn University, Auburn, AL. His dissertation work was in the area of microwave characterization and modeling of silicon-germanium heterojunction bipolar transistors.

In 1998, he joined the Microelectronics Division of IBM, East Fishkill, NY, where he is continuing to work with silicon-germanium and its applications in the personal communications market.

**Shiming Zhang** (S'99) was born in Beijing, China, in 1968. He received the B.E. degree in electrical engineering from Beijing Polytechnic University, China, in 1992. He is currently pursuing the M.S. degree in the Department of Electrical Engineering, Auburn University, Auburn, AL.

From 1992 to 1997, he worked on SiGe HBT in Beijing Polytechnic University as a Research Assistant. His main research interest is the RF and microwave characterization of SiGe HBT.

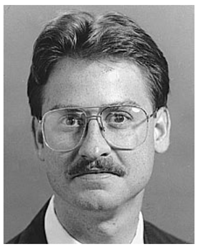

**John D. Cressler** (S'86–SM'91) received the B.S. degree in physics from the Georgia Institute of Technology, Atlanta, in 1984, and the M.S. and Ph.D. degrees in applied physics from Columbia University, New York, NY, in 1987 and 1990, respectively.

From 1984 to 1992, he was on the research staff at the IBM Research Division, Thomas J. Watson Research Center, Yorktown Heights, NY, where he worked in the Semiconductor Science and Technology Department on submicron silicon (Si) and silicon-germanium (SiGe) bipolar technology. His research interests at IBM included the physics and design of both ion-implanted and epitaxial Si and SiGe-base bipolar transistors and circuits, and particularly, the operation and understanding of such devices at cryogenic temperatures. In addition to his responsibilities while at IBM, he was an Adjunct Professor of Mathematics at Western Connecticut State University, Danbury, CT, from 1987 to 1990, as well as an Adjunct Assistant Professor of Electrical Engineering at Columbia University from 1990 to 1992. In 1992, he left the IBM Research Division to join the faculty of Auburn University, Auburn, AL. His research interests include SiGe HBT's and FET's, radiation effects, cryogenic electronics, SiC devices, RF/microwave circuits, reliability, noise, device simulation, and compact circuit modeling. He is currently Professor of Electrical Engineering and Assistant Director of the Alabama Microelectronics Science and Technology Center (AMSTC), a multidisciplinary, state-funded research center, and Director of the Cryogenic Electronics Laboratory within the AMSTC. He has published over 150 technical papers related to his research and written three book chapters. He has served as a consultant to IBM, Analog Devices, Westinghouse, ITRI/ERSO (Taiwan), Teltech, the National Technological University, Commercial Data Servers, and Texas Instruments.

Dr. Cressler received five awards from the IBM Research Division. He has served on the Technical Program Committees of the International Solid State Circuits Conference (1992–1998 and 1999–present), the Bipolar/BiCMOS Circuits and Technology Meeting (1995–present), and the International Electron Devices Meeting (1996–1997). He was the Technical Program Chairman of the 1998 ISSCC and is currently Chair of the Technology Directions subcommittee of the ISSCC. He is currently Chair of the Device Physics subcommittee of the BCTM and is also serving on the Executive Steering Committee for the IEEE Topical Meeting on Silicon Monolithic Integrated Circuits in RF Systems. He is an Associate Editor for the IEEE JOURNAL OF SOLID-STATE CIRCUITS (1998–present). He was appointed an IEEE Electron Devices Society Distinguished Lecturer in 1994. He was awarded the 1996 C. Holmes MacDonald National Outstanding Teacher Award by Eta Kappa Nu, the 1996 Auburn University Alumni Engineering Council Research Award, the 1998 Auburn University Birdsong Merit Teaching Award, the 1999 Auburn University Alumni Undergraduate Teaching Excellence Award, and the 1994 Office of Naval Research Young Investigator Award for his SiGe research program.

**Charles S. Webster** received the B.A. and M.S. degrees in physics from the University of Vermont, Burlington, in 1981 and 1985, respectively, and the M.S. degree in radiological physics/nuclear engineering science from the University of Florida, Gainesville, in 1995.

He is with IBM Microelectonics, Burlington, VT, where he is a member of the RF/Analog Development Group.

**Robert A. Groves** (M'94) received the B.S.E.E degree from the State University of New York in 1996.

He joined IBM Corporation, East Fishkill, NY, in 1989, where he worked as a Development Lab Technician, with an emphasis on high-frequency measurement and analysis. Since 1994, he has worked on SiGe technology development, with an emphasis on high-frequency characterization and modeling. His current interest is in microwave BEOL passive devices (interconnect, capacitors, and inductors), particularly integrated spiral inductor optimization and modeling.